JACS
JOURNAL OF THE AMERICAN CHEMICAL SOCIETY

ARTICLE

pubs.acs.org/JACS

Asymmetric Toggling of a Natural Photoswitch: Ultrafast Spectroscopy of Anabaena Sensory Rhodopsin

Amir Wand,[†] Rinat Rozin,[‡] Tamar Eliash,[‡] Kwang-Hwan Jung,[§] Mordechai Sheves,[‡] and Sanford Ruhman*[,†]

[†]Institute of Chemistry and Farkash Center for Light-Induced Processes, The Hebrew University of Jerusalem, Jerusalem 91904, Israel

[‡]Department of Organic Chemistry, The Weizmann Institute of Science, Rehovot 76100, Israel

[§]Department of Life Science and Institute of Biological Interfaces, Sogang University, Shinsu-Dong 1, Mapo-Gu, Seoul 121-742, South Korea

Supporting Information

ABSTRACT: Photochemistry in retinal proteins (RPs) is determined both by the properties of the retinal chromophore and by its interactions with the surrounding protein. The initial retinal configuration, and the isomerization coordinates active in any specific protein, must be important factors influencing the course of photochemistry. This is illustrated by the vast differences between the photoisomerization dynamics in visual pigments which start 11-*cis* and end all-*trans*, and those observed in microbial ion pumps and sensory rhodopsins which start all-*trans* and end in a 13-*cis* configuration. However, isolating these factors is difficult since most RPs accommodate only one active stable ground-state configuration. Anabaena sensory rhodopsin, allegedly functioning in cyanobacteria as a wavelength sensor, exists in two stable photoswitchable forms, containing all-*trans* and 13-*cis* retinal isomers, at a wavelength-dependent ratio. Using femtosecond spectroscopy, and aided by extraction of coherent vibrational signatures, we show that *cis*-to-*trans* photoisomerization, as in visual pigments, is ballistic and over in a fraction of a picosecond, while the reverse is nearly 10 times slower and kinetically reminiscent of other microbial rhodopsins. This provides a new test case for appreciating medium effects on primary events in RPs.

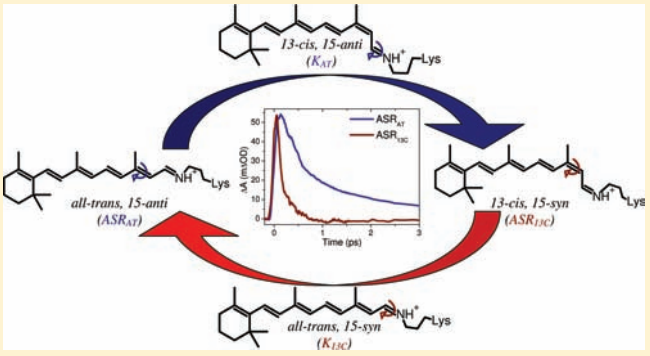

INTRODUCTION

The striking differences in photochemical dynamics between the visual pigments and their relatives, the microbial retinal proteins (MRPs), have puzzled photobiologists for decades. Both share similar architectures, and biological activity is fueled in both by photoisomerization of a retinal attached covalently to the protein via a protonated Schiff base (RPSB).[1,2] Despite this, absorption of light in the former has been shown by ultrafast spectroscopy to unleash ballistic sub-picosecond internal conversion (IC),[3−6] as demonstrated recently using high time-resolution hyper-spectral probing.[7] MRPs, in contrast, undergo crossing to the ground state roughly 10 times slower, apparently experiencing obstacles en route to photoisomerization. These allegedly induce multiexponential IC kinetics and spectral stagnation of the decaying excited state,[8−18] observed in solutions of RPSB as well.[19−23] Identifying the factors which govern this schism between the two divisions of retinal proteins (RPs) has attracted the attention of experimentalists and theorists alike.

An obvious possibility is that these differences stem from the retinal photoisomerization coordinate active in each case, all-*trans* to 13-*cis* in the microbial proteins[1] vs 11-*cis* to all-*trans* for the visual pigments. Indeed, a comparison of IC kinetics in all-*trans*, 13-*cis*, and 11-*cis* RPSB in solution has shown mild shortening of excited-state lifetimes in the latter two.[24,25] But this cannot be the whole story; First, this hastening falls short of explaining the acute variation in dynamics observed for visual and microbial RPs. Furthermore, different MRPs vary significantly in photoisomerization rates and efficiencies, despite their common reaction coordinate.[4,8−18,26−29] Structural investigations show that the retinal group in rhodopsin is twisted and compressed in the protein pocket.[30−33] Theoretical studies have assigned its ballistic and nuclear coherent IC to this prestraining,[34,35] either by virtue of the initial geometry itself[36] or by protein "guidance" of IC dynamics.[37−40] In contrast, similar studies in bacteriorhodopsin (BR) show that both light- and dark-adapted forms (LA and DA, respectively) contain a nearly planar retinal moiety. Accordingly, excited -state potential landscapes which are flat in the Franck−Condon region with respect to torsional motions are envisioned for BR (with an all-trans ground-state retinal isomer),[41−43] presumably leading to a sluggish onset of the IC.[8−23] Some have even postulated potential barriers resulting from interplay of several excited potentials, which interfere with arrival at the crossing to the ground state.[11,44,45] The existence of such a small barrier is further supported by experimental observations.[46]

Received: September 5, 2011
Published: November 07, 2011

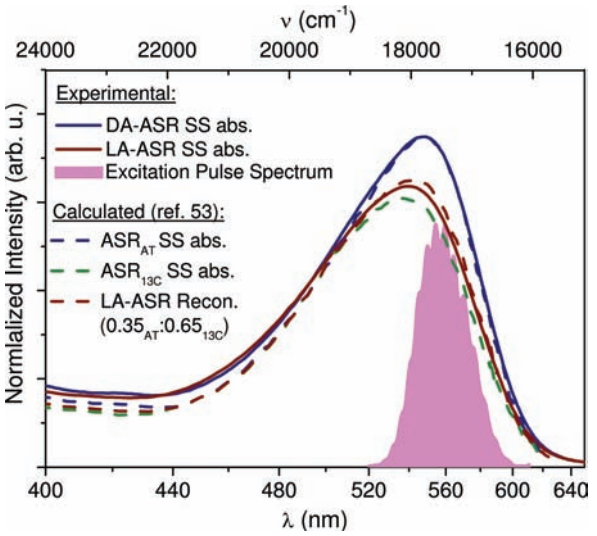

Figure 1. Experimental DA-ASR and LA-ASR steady-state absorption spectra, shown along with calculated ASR_{AT} and ASR_{13C} absorption spectra at 277 K.[53] A reconstruction of the LA-ASR absorption spectra by an adequate combination of the calculated ASR_{AT} and AST_{13C} spectra (0.35:0.65, respectively) is presented (see text and Supporting Information for details). TOPAS pump pulse spectrum is shown as well.

A recently discovered RP may cast new light on this issue. Anabaena sensory rhodopsin (ASR), unearthed through genome sequencing,[47,48] is found in the fresh-water cyanobacterium *Anabaena (Nostoc) sp.* PCC 7120.[47] ASR exhibits light-induced interconversion between two stable ground-state isomers of its retinal chromophore, 13-*cis*,15-*syn* (ASR_{13C}) and all-*trans*,15-*anti* (ASR_{AT}), depending on illumination wavelength. A hypsochromic shift of absorption on going from ASR_{AT} to ASR_{13C} causes the steady-state population ratio between these forms to depend on illumination wavelength (see spectra in Figure 1). Unlike other MRPs, but similar to visual pigments, ASR associates with a water-soluble protein, the ASR transducer (ASRT). Based on this state-specific affinity, it is believed to comprise a single-protein wavelength discrimination system, which regulates chromatic adaptation in the host bacterium.[47,49,50]

The bidirectional kinetics of ASR photoswitching, shown schematically in Figure 2, have been investigated by the groups of Spudich and Kandori (see ref 51 and references cited therein). Like BR, the ASR can accommodate the retinal chromophore in both all-*trans*,15-*anti* (BR_{AT}/ASR_{AT}) and 13-*cis*,15-*syn* (BR_{13C}/ASR_{13C}) configurations. In BR, irradiation leads from a 1:1 mixture established in the dark to exclusive population of the former biologically relevant configuration (BR_{AT}), in a process called "light adaptation". Absorption of light by BR_{AT} leads to selective isomerization around the $C_{13}{=}C_{14}$ bond to a reactive 13-*cis*,15-*anti* form within 1 ps. This triggers a photocycle of ~10 ms, which ultimately restores the protein to BR_{AT} after expelling a single proton from the cytoplasm. Despite structural similarities with BR determined via X-ray scattering experiments,[49] HPLC analysis determined that ASR assumes the all-*trans*,15-*anti* conformation almost exclusively (>97%) in the dark, while light adaptation with orange light leads to a photostationary isomer mixture in which ASR_{13C} is enriched up to ~80%.[51,52]

Low-temperature UV−vis, FTIR, and nanosecond flash-photolysis methods proved that photoswitching in ASR is exclusive, takes nearly 100 ms (in the all-*trans*→13-*cis* direction),

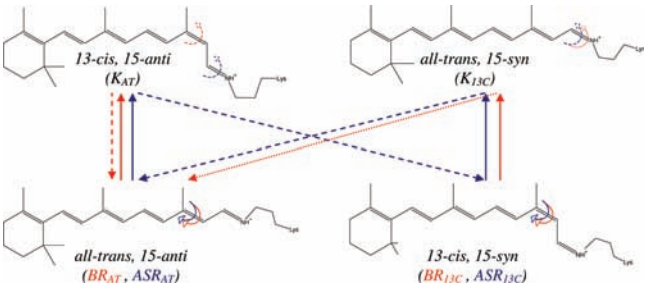

Figure 2. Photoinduced structural changes of the retinal chromophore in BR (red) and ASR (blue), including both possible initial states (X_{AT} and X_{13C}) and their corresponding photoproducts (K_{AT} and K_{13C}). Solid and dashed lines represent light-induced and thermal transformations, respectively.[51,82] The dotted arrow represents the light-adaptation process for BR, leading to accumulation of BR_{AT}.

and in both directions includes several distinct photointermediates.[51−54] The time scale for ASR_{AT} photoswitching is typical of sensory rhodopsins, and 1 order of magnitude slower than the proton pumping cycle in BR. The first of the photointermediates, coined "K", was contrasted with the corresponding photoreactant configuration using time-resolved FTIR-difference spectroscopy, showing that the light-induced structural changes in ASR_{AT} are fairly localized, while those following photolysis of ASR_{13C} are distributed widely along the polyene chain. It was further demonstrated that the rotational motion of the Schiff base upon retinal isomerization is probably smaller for ASR_{13C} than for ASR_{AT}.[55,56] The ~0.4 quantum yield for photoconversion from ASR_{AT} to ASR_{13C} was shown to be 1.5−3 times higher than that for the inverse process.[52,58]

ASR is thus a unique MRP featuring a *cis*-retinal photoreactant state alongside the common all-*trans* retinal form. Both retain protonation of the Schiff base, are apparently functional, and are perfectly photoswitchable.[53] This is highlighted in Figure 2, showing that photolyzed *cis* reactants terminate exclusively in the all-*trans* ground state, and vice versa.

Control over isomeric composition afforded by light and dark adaptation allows investigation of photoswitching dynamics in both directions, highlighting the effect of the initial retinal configuration on the photochemistry in a single protein, with minimal additional variations. To this end, we have initiated the first ultrafast laser experiment on the ASR. Sub 100-fs resolution transient spectra of DA-ASR and LA-ASR were recorded using pump−probe spectroscopy over a wide probing window from the visible to the NIR (~450−1450 nm). Separation of ASR_{13C} and ASR_{AT} contributions to LA-ASR data shows that *cis*-to-*trans* photoisomerization is ballistic and over in a fraction of a picosecond, as in visual pigments, while the reverse is nearly 10 times slower, and kinetically reminiscent of that of other MRPs. This provides a new model system for studying medium effects on primary events in RPs, raising the question of just how the opsin environment affects ASR photoswitching dynamics so differently in its two directions.

EXPERIMENTAL SECTION

Sample Preparation and Handling. ASR samples were prepared according to previously published methods.[47,57] ASR was expressed in *Escherichia coli* strain UT5600. *E. coli* transformants were grown in Luria−Bertani (LB) medium in the presence of ampicillin (100 μg/mL) at 37 °C. The cells were grown to A_{600} = 0.8, and induced with 1 mM IPTG and 10 μM all-*trans* retinal overnight. Pink-colored cells

were harvested by centrifugation and resuspended in 50 mM Tris-HCl buffer (pH 8), containing 300 mM NaCl, followed by centrifugation at 18 000 rpm for 5 min (4 °C). The precipitated cells were suspended with buffer S (50 mM 2-(*N*-morpholino)ethanesulfonic acid (MES), 300 mM NaCl, 5 mM imidazole, pH 6) containing 1% *n*-dodecyl-*β*-D-maltoside (DDM) and then lysed with lysozyme (0.1 mg/mL) in the presence of DNase at room temperature overnight. The extracted ASR protein was collected as supernatant after centrifugation at 18 000 rpm for 30 min (4 °C). The protein was purified by using a Ni^{2+}-NTA agarose column. The histidine-tagged protein was washed with buffer W (0.06% DDM, 50 mM MES, 300 mM NaCl, 50 mM imidazole, pH 6) and eluted with buffer E (0.06% DDM, 50 mM Tris-HCl, 300 mM NaCl, 50 mM HCl, 150 mM imidazole, pH 7.5). Eluted protein was washed and concentrated with phosphate buffer (50 mM, pH 7.5) containing 0.06% DDM, using Amicon ultracentrifugal filter devices.

Room-temperature samples with nominal optical density (OD) of ∼0.6 were syringe-pumped through a 0.4 mm path length cell, equipped with 0.15 mm fused silica windows. Sample integrity was determined spectrophotometrically before and after each run. DA-ASR samples were kept in the dark overnight and protected from photoconversion during experimental runs by eliminating photochemically effective ambient light. The maximum accumulated yield of laser-induced photoswitching from all-*trans* to ASR_{13C} during an experimental run was maintained below 15%.[58] LA-ASR was prepared by irradiation with an interference-filtered halogen lamp at 600 ± 35 nm (CORION P70-600-F) for ∼30 min, a procedure shown by HPLC analysis to generate a photostationary state.

HPLC. HPLC analysis was performed as previously described[59] with a few modifications. Retinal extraction was carried out under red light at room temperature. The samples were analyzed on a Purospher STAR Si-5 *μ*m (LichroCART 250-4, Merck) analytical column on a Waters 1525 HPLC equipped with a Waters 2487 dual-*λ* absorbance detector. The solvent was composed of 12% (v/v) ethyl acetate and 0.12% (v/v) ethanol in hexane, and the flow rate was 1.0 mL/min. Extraction of retinal oxime from the sample was carried out with hexane after addition of hydroxylamine (at least 1000-fold molar excess with respect to the pigment) and denaturation with ethanol. The molar compositions of the retinal isomers were calculated from the peak areas in the HPLC chromatograms. Assignment of the peaks was performed by comparing them with the HPLC pattern of retinal oximes extracted from DA- and LA-BR. DA samples were prepared by incubation in the dark for at least 24 h at room temperature. LA samples were prepared by illumination with Schott 250W cold light source (Carl Zeiss Microscopy, Jena, Germany) at 25 °C and using the CORION P70-600-F bandpass filter employed in pump−probe experiments. Retinal extraction was carried out under red light 0.5 min after the light adaptation to avoid any residual from transient intermediates.

Pump−Probe Experiments. The laser system and experimental layout, presented schematically in Figure S2 in the Supporting Information, have been described in detail elsewhere.[16] All experiments were based on homemade titanium−sapphire multipass amplifier systems, producing ∼30 fs pulses centered at 790 nm. Pulses of ∼25 fs duration and centered at 560 nm were obtained from a TOPAS optical parametric amplifier (Light Conversion, see Figure 1 for typical excitation spectrum), and a broadband supercontinuum probe was generated by focusing ∼1 *μ*J of the fundamental in 2.5 mm of sapphire.

For VIS (∼450−950 nm) probing, multifilament white light continuum pulses were split into probe and reference beams, and the former collimated and refocused into the sample with reflective optics. A 50 nJ pump beam was focused to a spot 200 *μ*m in diameter and overlapped with the probe, which was nearly 2 times smaller. The probe and reference pulses were directed through fibers to a double diode array spectrograph setup to generate a 512 pixel absorption spectrum. Such spectra were taken with and without pump, and subtraction of these provided wavelength-dependent ΔOD. Signal amplitudes were demonstrated to be linear in pump intensity up to 2 times that used in experiments. Due to detector limitations, two different scans were performed in the spectral regions of 450−850 and 550−950 nm, and then combined by adjusting the origin of delay to yield the best correspondence, as marked in Figure 3A using vertical lines.

In the NIR (∼900−1700 nm), a single-filament supercontinuum probe was refocused with reflective optics into the sample through a visible cutoff filter and then dispersed in an InGaAs array spectrograph (BTC261E, B&W TEK, USA). Consecutive pump-on and pump-off pulses were averaged and used to calculate the presented ΔOD.

For experiments in both probing regions, dispersion of pump pulses was compensated for in a slightly misaligned zero-dispersion grating pulse shaper, which also allowed truncation of pump spectral wings in order to reduce the effects of scattering. The obtained spectra were time-corrected for group dispersion of the probe continuum based on Kerr scans in water, which aside from providing the probe's *λ*-dependent group delay also indicated pump−probe cross-correlations of 70−90 and 50−70 fs for the VIS and NIR ranges, respectively.[60] To do this, the probe group delay dispersion (GDD), measured by optical Kerr effect, was fit to the group delay of a linear combination of sapphire and fused silica and used as the basis for time-correcting the transient absorption data sets. The spectral cuts of the data were then interpolated and shuffled in time to match the parametrized GDD. All data presented have undergone this correction.

RESULTS AND ANALYSIS

Isomeric Composition of the Samples. HPLC measurements proved that our LA-ASR sample was composed of 63 ± 3% 13-*cis* and 37 ± 3% all-*trans* isomers (pH 7.5), while DA-ASR contained 3 ± 1% 13-*cis* and 97 ± 1% all-*trans* isomers (see Figure S3 in the Supporting Information for details). This was verified to be compatible with the steady-state absorption of the samples by comparison to the spectra reported by Kawanabe et al.[53] (see Figure 1). The details can be found in Figure S4 in the Supporting Information. Briefly, the DA-ASR spectrum was almost indistinguishable from that of ASR_{AT} and was determined to be composed of 97 ± 3% ASR_{AT}. The LA-ASR reconstruction procedure was fraught with large uncertainties, and therefore our HPLC-determined ratio was adopted as a reference. It is shown to be compatible with the published absorption spectrum within reasonable experimental error. Accordingly, we assume that the DA-ASR and LA-ASR used in these experiments are composed of ∼100% and ∼35% ASR_{AT}, respectively.

Ultrafast Pump−Probe Data. The results of a single femtosecond pump−hyperspectral probe experiment consist of an $N \times M$ matrix of absorbance changes or ΔOD values at N probe wavelengths and M time delays: $\Delta OD(\lambda,t)$. ΔOD captures the spectral changes induced by the pump pulse as observed by the probe pulse impinging on the pumped samples at the designated time delays after the pump.[61] Accordingly, presenting the full data set requires a three-dimensional plot, λ and t as ordinate and coordinate, and ΔOD color-coded according to the attached scale or ruler. Pump-induced increases in absorption are coded in shades of orange to brown, while increased probe transmission is coded in shades of blue. Such representations of pump−probe data for DA-ASR and of LA-ASR are depicted in Figure 3A. The first 2 ps of delay are expanded to clarify the rapid spectral changes taking place during this period.

The gross appearance of transient spectral features is similar in both samples, exhibiting a rapid buildup of excited-state absorption and emission to the blue and to the red of the ∼550 nm ground-state bleach, respectively. Aside from some early spectral shifting, these features decay gradually within ∼5 ps, leaving

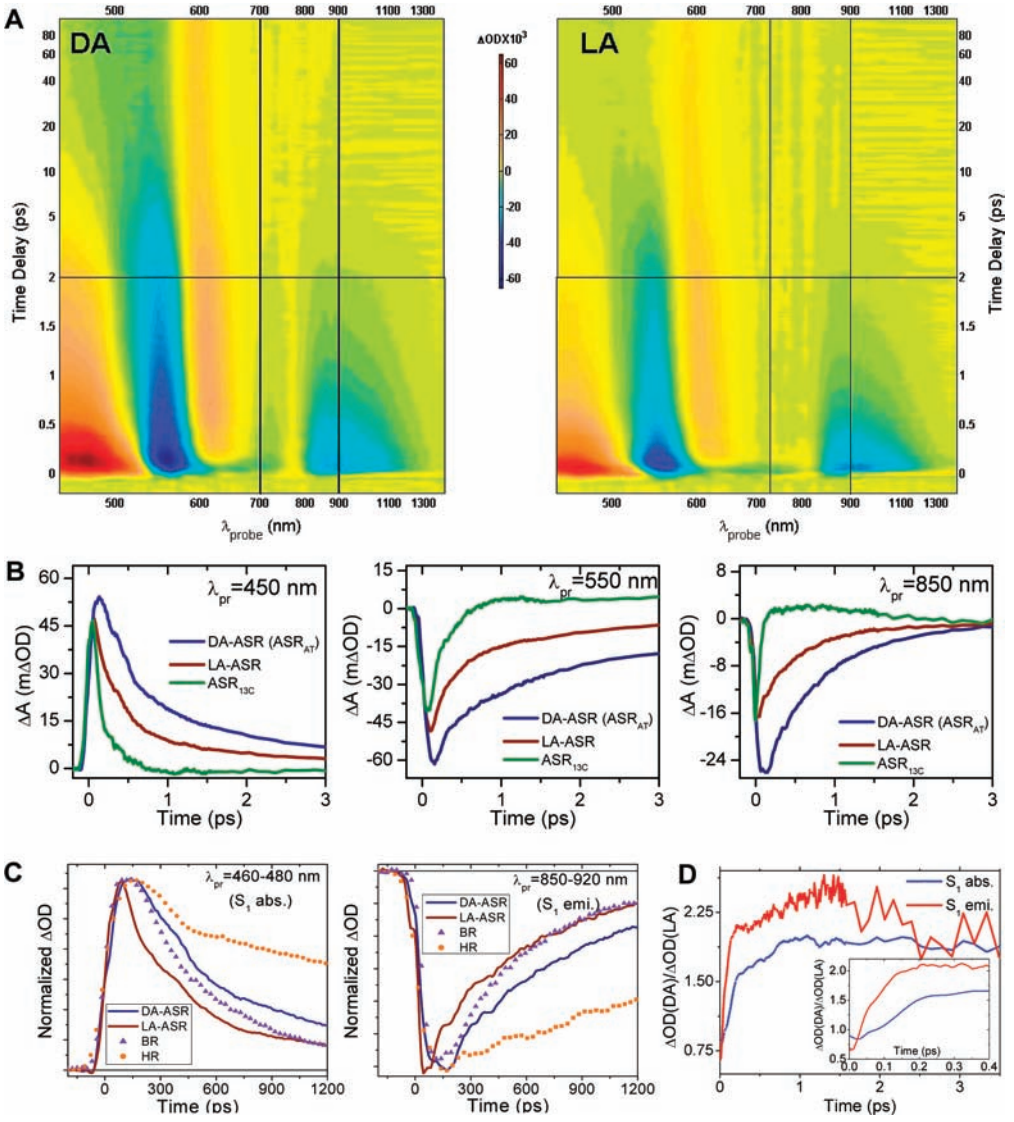

Figure 3. Transient ultrafast spectroscopy of Anabaena sensory rhodopsin. (A) Transient absorption differences for DA-ASR (left) and LA-ASR (right). The data are presented as color maps depicting the pump-induced difference of optical density (ΔOD, see color-bar inset) plotted against probe wavelength (horizontal axis) and pump−probe time delays (vertical axis). The delays are shown on a split time scale with an expanded scale up to 2 ps, and a logarithmic scale for longer times. The vertical lines depict regions of different data sets (see Experimental Section). (B) Spectral cuts (vertical cuts in the contour map of A) at three representative probing wavelengths of the transient difference spectra of DA-ASR (blue), LA-ASR (red), and ASR_{13C} (green), the third of which was derived by properly weighted subtraction of the former two (see Figure 9). These demonstrate the temporal evolution of the signal at a selected probe wavelength. (C) Short-time absorption changes for DA-ASR and LA-ASR (expanded scale of cuts like those in panel B), taken from this study, along with similar data for BR (from ref 11) and HR (from ref 16). (D) $\Delta OD_{DA}(t)/\Delta OD_{LA}(t)$ in the S_1 absorption band (450−470 nm) and emission band (820−850 nm). See text for details.

behind the weak signature of a red-shifted ground-state product ("K"), again apparent in both samples. These characteristics are reminiscent of similar data recorded for other MRPs, including BR, halorhodopsin (HR), and proteorhodopsin.[8−18] IC appears to take place with multiexponential kinetics within a few picoseconds. The NIR region presented up to 1450 nm exhibits a slow tapering of stimulated emission with λ_{probe}. A similar deep extension to low frequencies was recently reported for RPSB in ethanol.[62] Contrary to RPSB, however, no discernible absorptive signal was observed here deeper into the NIR. Another aspect of the data, which matches earlier studies on various MRPs, involves weak and rapidly decaying periodic modulations in the main difference spectral bands. These have been reported for BR, HR, and RPSB in solution, and attributed to impulsively excited coherent vibrational wavepackets in the fluorescent state (discussed later in the Vibrational Analysis section).

A closer look, however, reveals an early phase of rapid decay in excited-state features, showing up exclusively in the case of the LA-ASR data. This is even clearer in the spectral cuts shown in Figure 3B, where at all three representative wavelengths, an initial ∼0.5 ps decay is observed. The cuts in DA-ASR data, in contrast, exhibit an induction period in the decay of excited-state bands, similar to that observed in other MRPs, which like the DA-ASR start out with an all-*trans* retinal geometry (see Figure 3C).[11,16] This was also observed in all-*trans* RPSB in solution.[20,21] Beyond this point, spectral evolution in both samples appears similar,

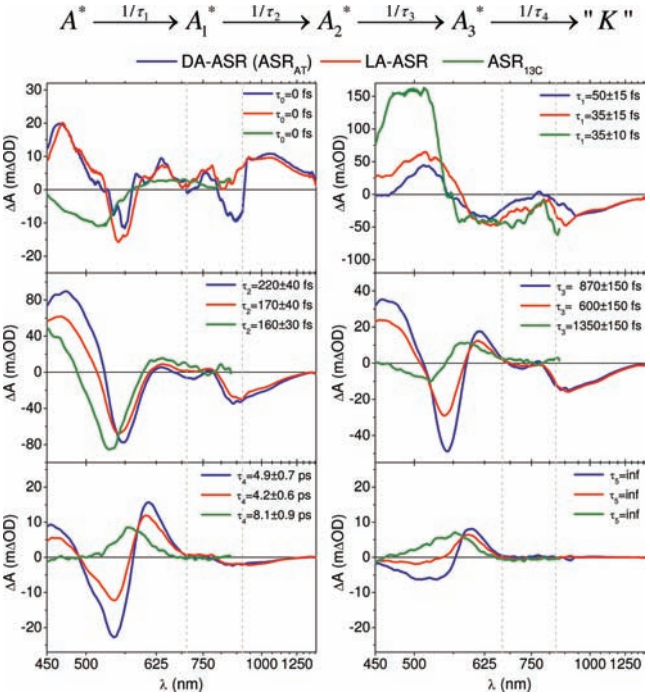

Figure 4. Evolutionary-associated decay spectra derived by global fitting to the sequential kinetic scheme above. The ASR_{13C} EADS were extracted by global fitting of a normalized, properly weighted subtraction of DA-ASR from LA-ASR data sets, which is shown in Figure 9 (see text for details).

aside from reduced amplitude of ΔOD for LA-ASR, presumably due to the described rapid decay. This is demonstrated by the leveling off of the ratio $[\Delta OD_{DA}(t)/\Delta OD_{LA}(t)]$ after $t \approx 0.5$ ps, shown in Figure 3D, an observation which will play a pivotal role in the interpretation and separation of isomeric contributions to the pump−probe data.

Target Analysis. To quantify the spectral evolution, global fitting was conducted with a sequential kinetic scheme:

$$A^* \xrightarrow{1/\tau_1} A_1^* \xrightarrow{1/\tau_2} A_2^* \xrightarrow{1/\tau_3} A_3^* \xrightarrow{1/\tau_4} K$$

yielding evolution-associated difference spectra (EADS) and matching decay times shown in Figure 4. A δ-function component representing coherent coupling of pump and probe during overlap was added, and the finite time resolution was accounted for by convolution with a Gaussian instrument response function (see Experimental Section for details). Fitting of the full data set was carried out iteratively. A preliminary fitting in the NIR spectral region was conducted to extract excited-state lifetimes, since this range is free of the spectral overlap with ground-state reactant and product spectra.[63] In accordance to previous studies on other RPs and on RPSB, a three-stage exponential decay model was found to provide an excellent fit to the data.[8−19] Time constants thus obtained were 40 ± 10, 340 ± 40, and 1000 ± 100 fs for DA-ASR, and 45 ± 10, 150 ± 30, and 720 ± 80 fs for LA sample. They were then used as an initial guess for global fitting in the visible.

Relative to the NIR, fitting the visible data requires at least one more step of evolution to account for the generation of a long-lived "K" intermediate, whose difference spectrum covers most of the visible. In fact, one more phase of spectral evolution was obtained, associated with a ∼5 ps exponential time constant, obviously due to a species not active in the NIR. This leads to a five-stage fitting scheme in the visible, not including the coherent coupling artifact. Addition of this instantaneous component led to superior fits of the data at short delays without noticeably affecting later EADS. Figure 4 presents the resulting EADS along with their corresponding lifetimes for DA-ASR (blue lines) and LA-ASR (red lines). The quality of reconstruction provided by the model is demonstrated in Figure S5 in the Supporting Information.

While the sub-picosecond EADS amplitudes for LA-ASR are as intense as, or even more so than those extracted from the DA sample, excited-state bands in the former diminish significantly in later stages of evolution. This is in line with the rapid decay discussed above. Furthermore, the decay times assigned to the picosecond stages of evolution, $\tau_{3,4}$, are virtually identical in both samples. This is in line with the leveling-off of the signal ratios after a fraction of a picosecond, as shown in Figure 3D. Finally, the "K" intermediate difference spectrum is qualitatively different in the two experiments, consisting of an increase in absorption almost throughout the whole probing range for LA-ASR, but exhibiting both positive and negative lobes in the case of DA-ASR. An interpretation of these results leading to a separation of 13-*cis* and all-*trans* isomer contributions to the LA-ASR data, based on the subtraction of a properly scaled replica of the DA signals, will be presented in the Discussion.

Vibrational Analysis. Periodical spectral modulations were extracted from the pump−probe data by subtracting the global fit from the raw data. Residuals were Fourier transformed in the time window 50 fs < t < 1500 fs, to obtain a power spectrum as described in ref 64. This procedure is demonstrated in Figure 5, which depicts its three stages for the case of DA-ASR probed at 820 nm, and was repeated for all wavelengths in both samples. As in other MRPs, the residuals and spectrograms show that the modulations are rapidly dephasing and limited to frequencies below 300 cm^{-1}, consistent with their arising from torsional excited-state motions in the retinal chromophore. While such signatures were discernible in LA and DA samples, they were clearer in the latter. Due to their low amplitude and rapid dephasing rates, only a rough central frequency of ∼160−180 cm^{-1} could be determined. Possible contributions from a number of distinct modes cannot be ruled out given the current signal-to-noise level.

Focusing on the stronger modulations extracted from the isomerically pure DA-ASR sample, the wavelength dependence of modulation phase and amplitude can be used to identify the electronic surfaces involved.[64−73] Figure 6 presents such an analysis: the upper panel depicts the intensity profile of the 160 cm^{-1} band as a function of probe wavelength, while below a set of residuals in the spectral region 700−820 nm is presented, offset vertically for clarity.

The wavelength dependence of the modulation pattern is consistent with its arising from motion in S_1, due to its bi-lobed intensity profile centered at ∼520 nm, which nearly coincides with the peak of the blue excited-state absorption band. This assignment is in line with previous experimental and theoretical studies of vibronic coherence signatures in other RPs.[13,16,21,42,45,74−79]

Further to the red, the double-humped intensity profile (Figure 6), along with the change of sign (π-phase jump) in the ∼200 fs period modulations around ∼740 nm, point to modulation of a band centered near that wavelength. Using the absolute phase of the modulation as a criterion for assignment leads to inconclusive results. As in the case of the modulations of *Hb. pharaonis* halorhodopsin (pHR) in a previous report (see Figure 4 in ref 16), excess absorption

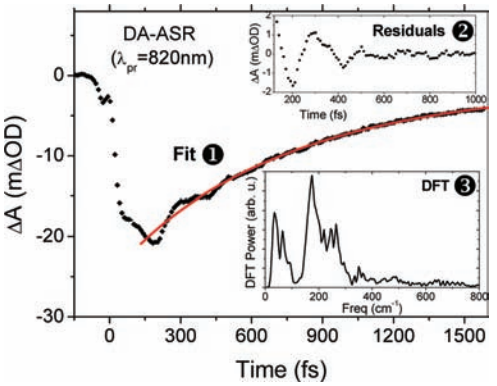

Figure 5. Demonstration of the analysis procedure used for the extraction of vibrational data from the pump−probe scans, shown as an example for the pump−probe data of DA-ASR at λ_{pr} = 820 nm. The multiexponential fit of the data (obtained from the EADS) is subtracted from the raw data (1) to obtain the residuals (2). These residuals are then discrete Fourier transformed to obtain the frequency-domain data (3).

is observed in the spectral part blue-shifted to that peak, and excess emission is observed in the red-shifted part. This would argue against these modulations originating from the NIR emission band, since that would lead to an initial Stokes shift, contrary to the observed trends. This may implicate the NIR absorption band instead. In any case, the amplitude spectrum and frequency of these modulations allow a confident assignment of their origin to coherently excited torsions in S_1.

Limitation of the detected coherences to low-frequency torsions must in part stem from the pulse durations used, allowing wave packet generation only in modes whose periods are significantly longer than the pump pulse duration. In an attempt to extract information on higher frequency vibrations accompanying excited-state evolution, ultrahigh temporal resolution (<10 fs) visible (500−700 nm) pump−probe experiments were conducted on the same samples (experimental details can be found in the Supporting Information and in ref 64). As in previous experiments on MRPs and RPSB in solution,[67,75,76,80] spectral modulations extracted from the data could be exclusively assigned to the ground state, generated by impulsive Raman excitation. Thus, no additional information concerning excited-state vibrational dynamics in higher frequency modes could be recovered. Instead, as detailed in Figure S6 in the Supporting Information, ground-state vibrational spectra obtained in this fashion verified the effectiveness of the light and dark adaptation protocols employed.

DISCUSSION

This is the first survey of primary light-induced events in Anabaena sensory rhodopsin, characterizing dynamics following excitation of either of its photobiological transformations, which together constitute the full photochromic cycle. It takes advantage of the unique coexistence of two biologically active reaction channels, associated with the two stable ground-state configurations. The objective was to further our understanding of how retinal conformation and protein interactions determine the photoreactivity of MRPs. This, however, requires a comparison of the dynamics unleashed by photoexcitation in ASR_{AT} to that in ASR_{13C}. While the former can be directly accessed by work on DA samples, extraction of the latter is more involved and requires further interpretation and manipulation of the data.

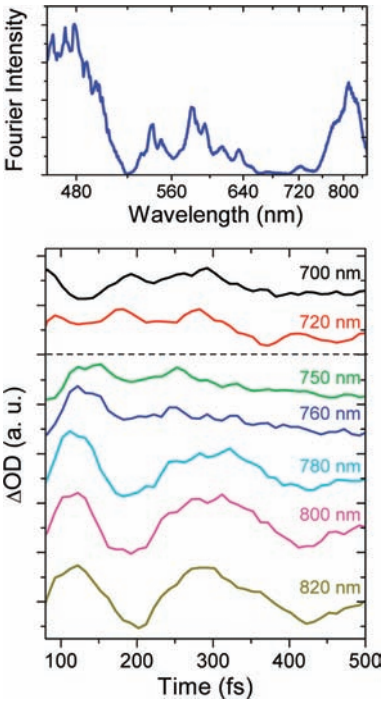

Figure 6. (Top) Intensity of modulations vs dispersed probe wavelength for the 160 cm^{-1} mode of the DA-ASR. (Bottom) Oscillatory residuals obtained after subtraction of the kinetic fits to the data (same as in Figure 5, see text for details) at a set of seven probing wavelengths in the range 700−820 nm for DA-ASR only. Curves are vertically translated to avoid overlapping. The horizontal dashed line is an estimate of the location of the phase reversal, corresponding to the peak of the relevant electronic band.

1. Interpretation of the Kinetic Analysis. Before addressing the differences between LA-ASR and DA-ASR photochemistry, we briefly discuss the features of the latter in comparison to other microbial RPs, sharing the same all-*trans* initial configuration. Having outlined the positions of ground-state bleach and excited-state absorption and emission features, in analogy with other MRPs,[8−18] the appearance of the EADS and their associated decay times serve to identify the processes underlying each. The sources of the $\delta(t)$-like nonlinear response, and of the long-lived photoproduct EADS, have already been identified. A_1*, which is associated with the second finite lifetime EADS, matches the transient difference spectrum of "I", the fluorescent state of BR, almost perfectly, exhibiting all three bands cited above. The gradual evolution from A_1* to "K" is characterized by intermediate difference spectra which can grossly be characterized as admixtures of both, with the "I" content diminishing as "K" accumulates. This speaks for all three stages, τ_2−τ_4, being dominated by gradual and nonexponential IC, leading to the first ground-state intermediate in both reaction channels.

Multiexponential IC kinetics, observed in virtually all RPs,[8−18,81] has been assigned alternately to bifurcation into several excited-state channels, to changes in rates of IC which arise from excited-state vibrational cooling, to inhomogeneities in protein structure, or to specific excited-state potential topologies.[12,14,15,44] The first of these is less likely in view of the results of stimulated-emission pumping experiments conducted on BR and pHR.[11,16] Whatever the mechanism is, current results demonstrate that IC is reasonably described as biexponential in ASR with either of the initial retinal

configurations. The requirement of a minor yet slower IC component for a perfect match to the measured kinetics demonstrates that biexponential descriptions are most likely approximating a more intricate continuous distribution of lifetimes, again arguing against the identification of each as a distinct reaction channel.[28]

Moving on to comparison between DA-ASR and LA-ASR dynamics, we note that both have similar general appearance, aside from the rapid initial phase of decay appearing exclusively in the latter during the initial ~300 fs of delay. This can be appreciated directly from the spectral cuts in Figure 3B, in the leveling-off of the DA-ASR over LA-ASR data (Figure 3D), and in the global fit analysis (Figure 4). Our interpretation of these results relies on the following assumptions: (1) The traces of ASR_{13C} present in DA-ASR can be ignored, and the DA sample is assumed to be pure ASR_{AT}. (2) In view of the similar intensity spectra of the pump laser and of the light adaptation lamp (see Supporting Information, Figure S1), we assume that the net photoswitching yield in LA-ASR is almost zero. This is ensured since forward and backward transitions must be balanced in the photostationary state. (3) The ratio of ASR_{AT}/ASR_{13C} photoswitching quantum yields is assumed to be 2, a rough average of different values reported in the literature.[52,58]

Keeping these in mind, two extreme scenarios depicted in Figure 7 were considered to explain the above observations. In the first, the rapid decay observed for LA-ASR is assumed to represent a *nonreactive* IC route, open only for the excited 13-*cis* isomer. Accordingly, the photoswitching itself takes place mainly on ~0.5 ps and longer time scales in both isomers. The second scenario envisions that IC and photoswitching in the 13-*cis* isomer of ASR are ultrafast, and complete in less than 1 ps. Accordingly, the later stages of decay, in both LA and DA samples, are due exclusively to slower IC of ASR_{AT}. The essential differences between the two schemes are that (a) in the first, both isomers, and not just ASR^*_{AT}, are contributing significantly to the spectral activity during $\tau_{3,4}$, (b) buildup of "K"$_{13C}$ should be complete in ~1 ps in scenario 2 but not in scenario 1, and (c) only scenario 1 requires early excited-state branching into distinct crossing points to the ground state.

These predictions allow quantitative testing of the data, which leads to the conclusion that the latter is far more likely to represent reality. Starting with the former, the assumption that reactive photoswitching takes place in both isomers on picosecond time scales, along with the identical picosecond decay times and associated difference spectra obtained in LA and DA-ASR, would require reactive IC to take place on precisely the same time scales in both ASR^*_{AT} and ASR^*_{13C}, and for both excited states to exhibit identical difference absorption spectra. This is extremely unlikely, providing grounds for ruling out scenario 1.

Demonstrating the likelihood of scenario 2 is aided by comparing dynamic difference spectra $[\Delta OD(t+\delta t) - \Delta OD(t)]$ obtained from both data sets, as exemplified in Figure 8 (see additional details in Figure S7 in the Supporting Information). This comparison for delays beyond $t \approx 0.8$ ps proves that such differences can be made to perfectly overlap by normalizing the spectra from LA- and DA-ASR experiments by a single scaling factor. This factor matches the HPLC-determined isomeric composition of the LA-ASR sample weighted by the relative extinction coefficients of ASR_{AT} and ASR_{13C}, lending further credibility to this scenario. This differencing procedure is necessary to compensate for the buildup of photoproduct from rapidly relaxing species, etc. The obtained match indicates that later stages of IC are due to one and the same species in both experiments, which can only be the excited ASR^*_{AT}.

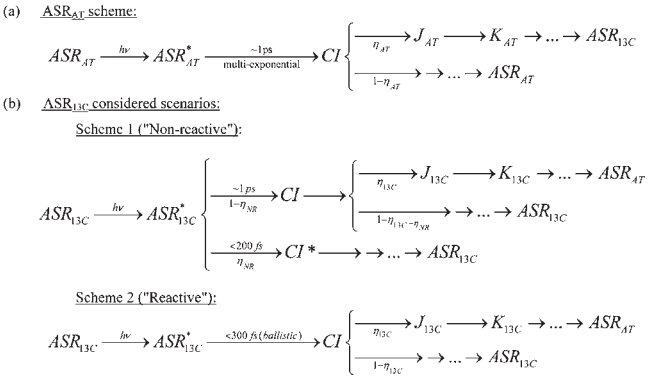

Figure 7. Possible schemes for the ultrafast photoreactions of both isomers of ASR. (a) Scheme for ASR_{AT} CI represents a conical intersection to the ground state, and η_{AT} the photoswitching yield. (b) The two scenarios for ASR_{13C} photoreactivity under consideration. Scheme 1 is the nonreactive one, where an ultrarapid (<200 fs) route leads η_{NR} of the population back to the ground state, leaving behind $(1 - \eta_{NR})$ undergoing a photocycle similar to that of ASR_{AT}. Note that the branching here takes place before reaching the "reactive" CI. Scheme 2 is the reactive one, describing ultrafast wavepacket-like reactive dynamics.

According to this interpretation, the contribution of ASR^*_{13C} to the transient spectra of LA-ASR can be isolated by subtracting a replica of the DA data set which produces identical dynamic difference spectra at long delays. As expected, the residual thus generated does exhibit a buildup of a photoproduct difference spectrum which closely resembles the published spectrum of "K"$_{13C}$, as can be seen in Figure 9 and in the corresponding EADS analysis presented in Figure 4 (green lines, shown only for the VIS probing spectral range). The contour mapping of the pure 13-*cis* ASR pump−probe data in Figure 9 is the most significant and extraordinary result of this study. It demonstrates how rapid IC of retinal is within the protein, when started in the 13-*cis*,15-*syn* configuration, in contrast to that shown in the left panel of Figure 3A (see also Figure S8).

This result is interesting, both in its magnitude and in its trend. Previous studies of RPSB photodynamics in proteins and in solution led to mixed predictions concerning the kinetics measured here. The slight shortening of excited-state lifetimes in 13-*cis* and 11-*cis* RPSB in organic solvents vs the all-*trans* compound[24] is marginal in view of the much stronger effects the opsin environment has on IC rates. Locking of specific double bonds to isomerization has had even more baffling results on IC rates of solvated RPSB molecules. Locking of the C_{13}═C_{14} double bond in either a *trans* or *cis* configuration has almost no effect on these rates,[13] while IC in chromophores locked in the 11-*cis* configuration is retarded nearly 10 times.[25] These results, thus, could not guide our expectations.

Factoring in opsin effects could be based on the details of retinal structure within the ASR as recorded by X-ray diffraction, in reference to the behavior of other MRPs which accommodate both retinal isomers, or through other measures indicating isomer-dependent strain or crowding in the protein pocket. The only X-ray diffraction study to date does not indicate significant changes, either in straining or in crowding of the RPSB, which could yield an educated guess concerning the IC rate ratio expected for the two forms of ASR.[49] This is also supported by a recent QM/MM theortical study of the ASR system.[82] In addition, resonance Raman measurements of the LA-ASR and DA-ASR do not point at any remarkable differences

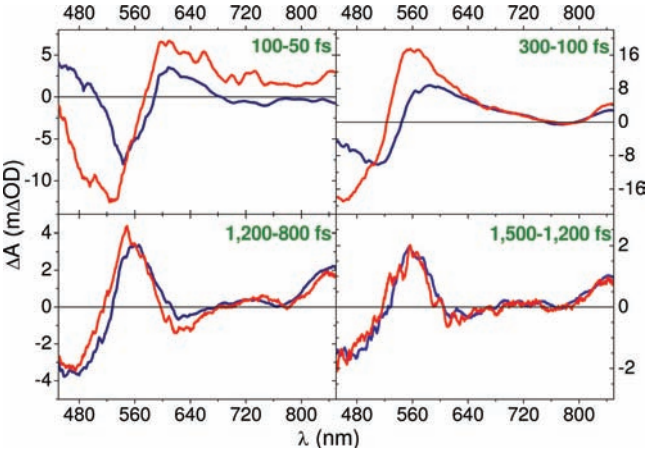

Figure 8. Four representative dynamic difference spectra $[\Delta OD(t+\delta t) - \Delta OD(t)]$ for DA-ASR (blue lines) and LA-ASR (red lines), with the former multiplied by a constant factor for all delays (the two time points designated in each panel correspond to $[t+\delta t]$ and $[t]$, respectively). This leads to nearly perfect overlaps for delays beyond ~0.8 ps, suggesting contribution from the same species in both samples. See more details in text and further dynamic difference spectra (also in the NIR probing region) in the Supporting Information (Figure S6).

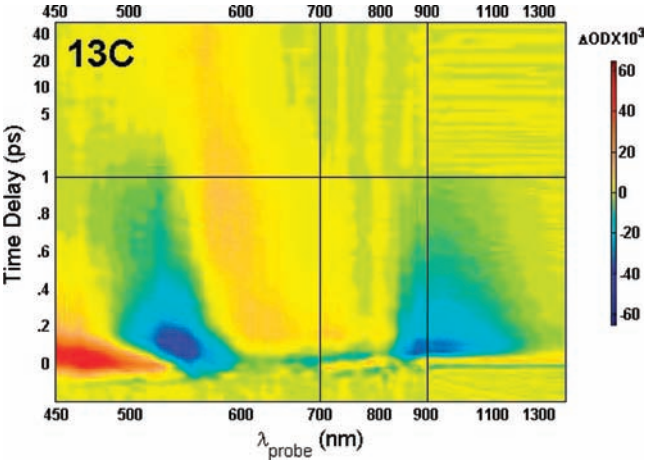

Figure 9. Normalized transient difference spectra obtained for ASR_{13C} by subtraction of properly weighted DA-ASR data from that obtained from LA-ASR (see text and Supporting Information for details). Representative spectral cuts of the contour maps are shown in Figure 3B.

in hydrogen out-of-plane modes,[54] which are known to be associated with prestraining or chromophore distortion in RPs. Similarly, the systematic blue-shifting and weakening in absorption following double bond isomerization of all-*trans* to 13-*cis* configurations of RPSB appear already in solution but have a negligible effect on IC kinetics. Accordingly, the spectral changes between ASR_{13C} and ASR_{AT} are not indicative of any unusual differences in straining of the chromophore in either of the stable variants.

The only experimental evidence which might explain this dynamic asymmetry in photoswitching comes from difference FTIR data showing that (a) upon retinal isomerization, the rotational motion of the Schiff base is smaller for ASR_{13C} relative to ASR_{AT}, (b) the structural changes upon creation of the K photoproduct are widely distributed along the polyene chain for ASR_{13C}, and localized near the Schiff-base for ASR_{AT}, and (c) in the case of ASR_{AT}, "K" intermediate formation involves stronger disruption of hydrogen bonds to the Schiff base, possibly introducing a potential barrier to isomerization specific to this direction of switching.[55,82] While reaction coordinates calculated for both switching directions were reported by Strambi et al., no conclusions concerning asymmetry in photoinduced dynamics were drawn.[82] In addition, since the rates of IC reflect the course of transition from the Franck−Condon state to the crossing points to the ground state, structural differences between the reactant and first ground-state photoproducts do not directly bear on the question at hand.

This leaves BR photochemistry as the most relevant experimental reference frame for generalizing the present observations. BR, like ASR, naturally accommodates both all-*trans* and the 13-*cis* isomers of RPSB in relaxed ground-state species, the latter appearing appreciably only in DA samples. The only comparative ultrafast study of both was performed by Petrich et al.[83] in 1987. Analysis of pump−probe data led the authors to conclude that no significant differences in IC kinetics exist between all-*trans* and 13-*cis* forms of BR. They also pointed out that, due to excitation wavelength restrictions, their pioneering study was limited in its sensitivity to the spectral contributions of the BR_{13C} component.

Thus, a more comprehensive study of LA- and DA-BR samples will be required to determine if the trends observed for ASR carry over to the BR as well. In any case, the current experimental results constitute the first experimental demonstration that, within the same protein, the 13-*cis*→all-*trans* photoisomerization is much faster than in the opposite switching direction. In addition, the reported stagnation phase frequently observed in the photochemistry of all-*trans* RPs (see Figure 3C), and absent in the 13-*cis* isomer of ASR, must be addressed in future theoretical studies of this protein as well.

2. Relevance to Other Retinal Proteins and Concluding Remarks. Aside from the inherent interest in characterizing ASR photochemistry, a prime incentive of our study was the ability to compare photodynamics of two biologically active retinal configurations within the same protein surroundings. We also hoped that, by analogy, the results would clarify the sources of the very different IC dynamics in type-1 rhodopsins and type-2 visual pigments. One previous effort to test variations in photoisomerization dynamics for different initial retinal configurations in the same RP involved a comparative study of rhodopsin and isorhodopsin. That study, however, compared the rates of two initial *cis* states: the visual pigment which consists of 11-*cis* retinal isomer with isorhodopsin characterized by a 9-*cis* retinal isomer, both leading to the same photointermediate. While the latter was found to undergo IC somewhat slower, tentatively associated with either different ground-state straining of the chromophore or a small barrier on the way to isomerization, it is not clear how this relates to our study, since it involves activity around two different double bonds.[84,85]

The current ultrafast spectroscopic investigation of LA-ASR and DA-ASR shows that, as in other MRPs (BR, HR, etc.), IC in the all-*trans* isomer takes place with multiexponential kinetics accompanied by low-frequency vibrational coherences in the excited state, detected as spectral modulations in absorption and emission of the fluorescent state. As demonstrated in Figure 3C, this similarity carries over also to the spectral stagnation observed in all these all-*trans* systems during the first ~100 fs of excited-state evolution.[11,16,19−21] This common feature may hark back to a similar potential topology in the Franck−Condon region of the all-*trans* RPSB.

In contrast, photoisomerization dynamics in the ASR_{13C} isomer are much faster, resembling ballistic wavepacket motion

akin to that in 11-*cis* visual pigments. At present, the signal-to-noise obtained after the subtraction of DA- from LA-ASR data does not allow a conclusive ruling on whether, as in the case of rhodopsin, this rapid process is accompanied by vibrational coherences in the photoproduct. In the latter, that observation was seen as another indicator for the ballistic nature of IC. As ASR is the only microbial RP with a biologically relevant *cis* retinal reactant state, the relevance of our findings to other MRPs is still unclear. The kinetic similarity of IC in ASR_{13C} to that in rhodopsin, despite the different protein surroundings, does however reiterate the question of whether the starting configuration itself, within any of the relevant RPs, suffices to generate such dynamics for crossing to the ground state. In this respect it is interesting to note that both rhodopsin and isorhodopsin start off in a *cis* retinal conformation, and although they differ in IC dynamics, in both cases a recent study reports vibrational coherence conservation in the photoproducts, and in both cases the overall IC durations are shorter than photoisomerization in most other MRPs, starting off all-*trans*.[86]

To conclude, the significance of our findings is profound. The vast dynamical differences observed, with none of the structural attributes held responsible for the dynamical contrasts between MRPs and visual pigments, call for revisions in rationalizing RP photochemistry. The application of time-dependent quantum chemistry to the dynamics of RPs is not a new field. However, simulations which model the protein explicitly require immense computing resources, which only recently have become available. Yet, building such models is a major effort, changing significantly from protein to protein. Thus, comparing simulated dynamics in different proteins suffers from an "oranges vs apples" aspect. Here, we present a new archetype for testing our understanding of RP dynamics and details of opsin effects within the same protein, enriching the discourse and tightening control of simulation methods used for this intriguing family of proteins. The fact that the discrepancy in rates is on the order of magnitude level promises that such a comparison will not be whittled down to a pittance within significant margins of error. Realistic computer simulations should thus not only explain why ASR photoswitching dynamics in both directions are so dissimilar but alos, by comparison, allow a deeper appreciation of the factors governing the course of photoisomerization in other RPs as well.

■ ASSOCIATED CONTENT

Supporting Information. Further information on materials and methods, determination of the LA-ASR isomeric composition, demonstration of the goodness of the global fitting process, high temporal resolution impulsive vibrational spectroscopy results, dynamic difference spectra analysis procedure, direct comparison of ASR_{AT} and ASR_{13C} transient spectra (Figures S1−S8 and references), and complete ref 48. This material is available free of charge via the Internet at http://pubs.acs.org.

■ AUTHOR INFORMATION

Corresponding Author
sandy@fh.huji.ac.il

■ ACKNOWLEDGMENT

This work was supported by the Israel Science Foundation, which is administered by the Israel Academy of Sciences and Humanities, US-Israel Binational Science Foundation, and NRF of Korea 2011-0012320. A.W. is supported by the Adams Fellowship Program of the Israel Academy of Sciences and Humanities. M.S. holds the Katzir-Makineni chair in chemistry. The Farkas Center for Light-Induced Processes is supported by the Minerva-Gesellschaft für die Forschung GmbH, München, Germany.

■ REFERENCES

(1) Spudich, J. L.; Yang, C.-S.; Jung, K.-H.; Spudich, E. N. *Annu. Rev. Cell Dev. Biol.* **2000**, *16*, 365–392.
(2) Spudich, J. L.; Jung, K.-H. Microbial rhodopsins: phylogenetic and functional diversity. In *Handbook of Photosensory Receptors*; Briggs, W. R., Spudich, J. L, Eds.; Wiley-VCH: Weinheim, 2005; pp 1−24.
(3) Schoenlein, R. W.; Peteanu, L. A.; Mathies, R. A.; Shank, C. V. *Science* **1991**, *254*, 412–415.
(4) Kochendoerfer, G. G.; Mathies, R. A. *Isr. J. Chem.* **1995**, *35*, 211–226.
(5) Haran, G.; Morlino, E. A.; Matthes, J.; Callender, R. H.; Hochstrasser, R. M. *J. Phys. Chem. A* **1999**, *103*, 2202–2207.
(6) Kandori, H.; Furutani, Y.; Nishimura, S.; Shichida, Y.; Chosrowjan, H.; Shibata, Y.; Mataga, N. *Chem. Phys. Lett.* **2001**, *334*, 271–276.
(7) Polli, D.; Altoe, P.; Weingart, O.; Spillane, K. M.; Manzoni, C.; Brida, D.; Tomasello, G.; Orlandi, G.; Kukura, P.; Mathies, R. A.; Garavelli, M.; Cerullo, G. *Nature* **2010**, *467*, 440–443.
(8) Mathies, R. A.; Cruz, C. H. B.; Pollard, W. T.; Shank, C. V. *Science* **1988**, *240*, 777–779.
(9) Dobler, J.; Zinth, W.; Kaiser, W.; Oesterhelt, D. *Chem. Phys. Lett.* **1988**, *144*, 215–220.
(10) Kobayashi, T.; Terauchi, M.; Kouyama, T.; Yoshizawa, M.; Taiji, M. *Proc. SPIE* **1991**, *1403*, 407–416.
(11) Ruhman, S.; Hou, B.; Friedman, N.; Ottolenghi, M.; Sheves, M. *J. Am. Chem. Soc.* **2002**, *124*, 8854–8858.
(12) Gai, F.; Hasson, K. C.; McDonald, J. C.; Anfinrud, P. A. *Science* **1998**, *279*, 1886–1891.
(13) Hou, B.; Friedman, N.; Ottolenghi, M.; Sheves, M.; Ruhman, S. *Chem. Phys. Lett.* **2003**, *381*, 549–555.
(14) Arlt, T.; Schmidt, S.; Zinth, W.; Haupts, U.; Oesterhely, D. *Chem. Phys. Lett.* **1995**, *241*, 559–565.
(15) Nakamura, T.; Takeuchi, S.; Shibata, M.; Demura, M.; Kandori, H.; Tahara, T. *J. Phys. Chem. B* **2008**, *112*, 12795–12800.
(16) Bismuth, O.; Komm, P.; Friedman, N.; Eliash, T.; Sheves, M.; Ruhman, S. *J. Phys. Chem. B* **2010**, *114*, 3046–3051.
(17) Lutz, I.; Sieg, A.; Wegener, A. A.; Engelhard, M.; Boche, I.; Otsuka, M.; Oesterhelt, D.; Wachtveitl, J.; Zinth, W. *Proc. Natl. Acad. Sci. U.S.A.* **2001**, *98*, 962–967.
(18) Amsden, J. J.; Kralj, J. M.; Chieffo, L. R.; Wang, X.; Erramilli, S.; Spudich, E. N.; Spudich, J. L.; Ziegler, L. D.; Rothschild, K. J. *J. Phys. Chem. B* **2007**, *111*, 11824–11831.
(19) (a) Hamm, P.; Zurek, M.; Roschinger, T.; Patzelt, H.; Oesterhelt, D.; Zinth, W. *Chem. Phys. Lett.* **1996**, *263*, 613–621. (b) Hamm, P.; Zurek, M.; Roschinger, T.; Patzelt, H.; Oesterhelt, D.; Zinth, W. *Chem. Phys. Lett.* **1997**, *268*, 180–186.
(20) Bismuth, O.; Friedman, N.; Sheves, M.; Ruhman, S. *Chem. Phys.* **2007**, *341*, 267–275.
(21) Zgrablić, G.; Voïtchovsky, K.; Kindermann, M.; Haacke, S.; Chergui, M. *Biophys. J.* **2005**, *88*, 2779–2788.
(22) Hou, B.; Friedman, N.; Ruhman, S.; Sheves, M.; Ottolenghi, M. *J. Phys. Chem. B* **2001**, *105*, 7042–7048.
(23) Kandori, H.; Sasabe, H. *Chem. Phys. Lett.* **1993**, *216*, 126–132.
(24) Logunov, S. L.; Song, L.; El-Sayed, M. *J. Phys. Chem.* **1996**, *100*, 18586–18591.
(25) Kandori, H.; Katsuta, Y.; Ito, M.; Sasabe, H. *J. Am. Chem. Soc.* **1995**, *117*, 2669–2670.
(26) (a) Lenz, M. O.; Huber, R.; Schmidt, B.; Gilch, P.; Kalmbach, R.; Engelhard, M.; Wachtveitl, J. *Biophys. J.* **2006**, *91*, 255–262. (b) Rupenyan, A.;

van Stokkum, I. H. M.; Arents, J. C.; van Grondelle, R.; Hellingwerf, K.; Groot, M. L. *Biophys. J.* **2008**, *94*, 4020–4030. (c) Neumann, K.; Verhoefen, M.-K.; Weber, I.; Glaubitz, C.; Wachtveitl, J. *Biophys. J.* **2008**, *94*, 4796–807.

(27) (a) Govindjee, R.; Balashov, S. P.; Ebrey, T. G. *Biophys. J.* **1990**, *58*, 597–608. (b) Logunov, S. L.; El-Sayed, M. A. *J. Phys. Chem. B* **1997**, *101*, 6629–6633. (c) Kim, J. E.; Tauber, M. J.; Mathies, R. A. *Biochemistry* **2001**, *40*, 13774–13778. (d) Losi, A.; Wegener, A. A.; Engelhard, M.; Braslavsky, S. E. *Photochem. Photobiol.* **2001**, *74*, 495–503.

(28) Briand, J.; Léonard, J.; Haacke, S. *J. Opt.* **2010**, *12*, 084004.

(29) Kobayashi, T.; Kim, M.; Taiji, M.; Iwasa, T.; Nakagawa, M.; Tsuda, M. *J. Phys. Chem. B* **1998**, *102*, 272–280.

(30) Smith, S. O.; Palings, I.; Copie, V.; Raleigh, D. P.; Courtin, J.; Pardoen, J. A.; Lugtenburg, J.; Mathies, R. A.; Griffin, R. G. *Biochemistry* **1987**, *26*, 1606–1611.

(31) Palings, I.; Pardoen, J. A.; Vandenberg, E.; Winkel, C.; Lugtenburg, J.; Mathies, R. A. *Biochemistry* **1987**, *26*, 2544–2556.

(32) Kochendoerfer, G.; Verdegem, P. J. E.; van der Hoef, I.; Lugtenburg, J.; Mathies, R. A. *Biochemistry* **1996**, *35*, 16230–16240.

(33) Brown, M. F.; Heyn, M. P.; Job, C.; Kim, S.; Moltke, S.; Nakanishi, K.; Nevzorov, A. A.; Struts, A. V.; Salgado, G. F. J.; Wallat, I. *Biochim. Biophys. Acta* **2007**, *1768*, 2979–3000.

(34) Sugihara, M.; Hufen, J.; Buss, V. *Biochemistry* **2006**, *45*, 801–810.

(35) (a) Ben-Nun, M.; Molnar, F.; Schulten, K.; Martínez, T. J. *Proc. Natl. Acad. Sci. U.S.A.* **2002**, *99*, 1769–1773. (b) Virshup, A. M.; Punwong, C.; Pogorelov, T. V.; Lindquist, B. A.; Ko, C.; Martínez, T. J. *J. Phys. Chem. B* **2009**, *113*, 3280–3291.

(36) Weingart, O.; Schapiro, I.; Buss, V. *J. Phys. Chem. B* **2007**, *111*, 3782–3788.

(37) Tomasello, G.; Olaso-Gonzalez, G.; Altoe, P.; Stenta, M.; Serrano-Andres, L.; Merchan, M.; Orlandi, G.; Bottoni, A.; Garavelli, M. *J. Am. Chem. Soc.* **2009**, *131*, 5172–5186.

(38) Hayashi, S.; Tajkhorshid, E.; Schulten, K. *Biophys. J.* **2009**, *96*, 403–416.

(39) Cembran, A.; González-Luque, R.; Serrano-Andrés, L.; Merchán, M.; Garavelli, M. *Theor. Chem. Acc.* **2007**, *118*, 173–183.

(40) Li, X.; Chung, L. W.; Morokuma, K. *J. Chem. Theory Comput.* **2011**, *7*, 2694–2698.

(41) Garavelli, M.; Vreven, T.; Celani, P.; Bernardi, F.; Robb, M. A.; Olivucci, M. *J. Am. Chem. Soc.* **1998**, *120*, 1285–1288.

(42) Cembran, A.; Bernardi, F.; Olivucci, M.; Garavelli, M. *J. Am. Chem. Soc.* **2003**, *125*, 12509–12519.

(43) Hayashi, S.; Tajkhorshid, E.; Schulten, K. *Biophys. J.* **2003**, *85*, 1440–1449.

(44) Olivucci, M.; Lami, A.; Santoro, F. *Angew. Chem., Int. Ed.* **2005**, *44*, 5118–5121.

(45) Hasson, K. C.; Gai, F.; Anfinrud, P. A. *Proc. Natl. Acad. Sci. U.S.A.* **1996**, *93*, 15124–15129.

(46) (a) Alfano, R. R.; Yu, W.; Govindjee, R.; Becher, B.; Ebrey, T. G. *Biophys. J.* **1976**, *16*, 541–545. (b) Shapiro, S. L.; Campillo, A. J.; Lewis, A.; Perreault, G. J.; Spoonhower, J. P.; Clayton, R. K.; Stoeckenius, W. *Biophys. J.* **1978**, *23*, 383–393.

(47) Jung, K.-H.; Trivedi, V. D.; Spudich, J. L. *Mol. Microbiol.* **2003**, *47*, 1513–1522.

(48) Venter, J. C.; et al. *Science* **2004**, *304*, 66–74.

(49) Vogeley, L.; Sineshchekov, O. A.; Trivedi, V. D.; Sasaki, J.; Spudich, J. L.; Luecke, H. *Science* **2004**, *306*, 1390–1393.

(50) Kondoh, M.; Inoue, K.; Sasaki, J.; Spudich, J. L.; Terazima, M. *J. Am. Chem. Soc.* **2011**, *133*, 13406–13412.

(51) Kawanabe, A.; Kandori, H. *Sensors* **2009**, *9*, 9741–9804.

(52) Sineshchekov, O. A.; Trivedi, V. D.; Sasaki, J.; Spudich, J. L. *J. Biol. Chem.* **2005**, *280*, 14663–14668.

(53) Kawanabe, A.; Furutani, Y.; Jung, K.-H.; Kandori, H. *J. Am. Chem. Soc.* **2007**, *129*, 8644–8649.

(54) Shi, L.; Yoon, S. R.; Bezerra, A. G.; Jung, K.-H.; Brown, L. S. *J. Mol. Biol.* **2006**, *358*, 686–700.

(55) (a) Furutani, Y.; Kawanabe, A.; Jung, K.-H.; Kandori, H. *Biochemistry* **2005**, *44*, 12287–12296. (b) Kawanabe, A.; Furutani, Y.; Jung, K.-H.; Kandori, H. *Biochemistry* **2006**, *45*, 4362–4370. (c) Kawanabe, A.; Furutani, Y.; Yoon, S. R.; Jung, K.-H.; Kandori, H. *Biochemistry* **2008**, *47*, 10033–10040.

(56) Bergo, V. B.; Ntefidou, M.; Trivedi, V. D.; Amsden, J. J.; Kralj, J. M.; Rothschild, K. J.; Spudich, J. L. *J. Biol. Chem.* **2006**, *281*, 15208–15214.

(57) Choi, A. R.; Kim, S. Y.; Yoon, S. R.; Bae, K.; Jung, K.-H. *J. Microbiol. Biotechnol.* **2007**, *17*, 138–145.

(58) Wada, Y.; Kawanabe, A.; Furutani, Y.; Kandori, H. *Chem. Phys. Lett.* **2008**, *453*, 105–108.

(59) Shimono, K.; Ikeura, Y.; Sudo, Y.; Iwamoto, M.; Kamo, N. *Biochim. Biophys. Acta* **2001**, *1515*, 92–100.

(60) Polli, D.; Brida, D.; Mukamel, S.; Lanzani, G.; Cerullo, G. *Phys. Rev. A* **2010**, *82*, 053809.

(61) Cerullo, G.; Manzoni, C.; Lüer, L.; Polli, D. *Photochem. Photobiol. Sci.* **2007**, *6*, 135–144.

(62) Loevsky, B.; Wand, A.; Bismuth, O.; Friedman, N.; Sheves, M.; Ruhman, S. *J. Am. Chem. Soc.* **2011**, *133*, 1626–1629.

(63) Kahan, A.; Wand, A.; Ruhman, S.; Zilberg, S.; Haas, Y. *J. Phys. Chem. A* **2011**, *115*, 10854–10861.

(64) Wand, A.; Kallush, S.; Shoshanim, O.; Bismuth, O.; Kosloff, R.; Ruhman, S. *Phys. Chem. Chem. Phys.* **2010**, *12*, 2149–2163.

(65) *Coherent Vibrational Dynamics*; De-Silvestri, S., Cerullo, G., Lanzani, G., Eds.; CRC Press: Boca Raton, FL, 2008.

(66) (a) Kumar, A. T. N.; Rosca, F.; Widom, A.; Champion, P. M. *J. Chem. Phys.* **2001**, *114*, 701–724. (b) Kumar, A. T. N.; Rosca, F.; Widom, A.; Champion, P. M. *J. Chem. Phys.* **2001**, *114*, 6795–6815.

(67) Pollard, W. T.; Fragnito, H. L.; Bigot, J.-Y.; Shank, C. V.; Mathies, R. A. *Chem. Phys. Lett.* **1990**, *168*, 239–245.

(68) Pollard, W. T.; Dexheimer, S. L.; Wang, Q.; Peteanu, L. A.; Shank, C. V.; Mathies, R. A. *J. Phys. Chem.* **1992**, *96*, 6147–6158.

(69) Dobryakov, A. L.; Ernsting, N. P. *J. Chem. Phys.* **2008**, *129*, 184504.

(70) Cirmi, G.; Brida, D.; Gambetta, A.; Piacenza, M.; Sala, F. D.; Favaretto, L.; Cerullo, G.; Lanzani, G. *Phys. Chem. Chem. Phys.* **2010**, *12*, 7917–7923.

(71) (a) Bardeen, C. J.; Wang, Q.; Shank, C. V. *J. Phys. Chem. A* **1998**, *102*, 2759–2766. (b) Bardeen, C. J.; Wang, Q.; Shank, C. V. *Phys. Rev. Lett.* **1995**, *75*, 3410–3413.

(72) (a) Banin, U.; Waldman, A.; Ruhman, S. *J. Chem. Phys.* **1992**, *96*, 2416–2419. (b) Banin, U.; Ruhman, S. *J. Chem. Phys.* **1993**, *98*, 4391–4403. (c) Banin, U.; Bartana, A.; Ruhman, S.; Kosloff, R. *J. Chem. Phys.* **1994**, *101*, 8461–8481. (d) Gershgoren, E.; Vala, J.; Kosloff, R.; Ruhman, S. *J. Phys. Chem. A* **2001**, *105*, 5081–5095.

(73) Lüer, L.; Gadermaier, C.; Crocher, J.; Hertel, T.; Brida, D; Lanzani, G. *Phys. Rev. Lett.* **2009**, *102*, 127401.

(74) Lin, S. W.; Groesbeek, M.; van der Hoef, I.; Verdegem, P.; Lugtenburn, J.; Mathies, R. A. *J. Phys. Chem. B* **1998**, *102*, 2787–2806.

(75) Kahan, A.; Nahmias, O.; Friedman, N.; Sheves, M.; Ruhman, S. *J. Am. Chem. Soc.* **2007**, *129*, 537–546.

(76) (a) Kraack, J. P.; Buckup, T.; Hampp, N.; Motzkus, M. *ChemPhysChem* **2011**, *12*, 1851–1859. (b) Kraack, J. P.; Buckup, T.; Motzkus, M. *Phys. Chem. Chem. Phys.* **2011**, DOI: 10.1039/C1CP22245G.

(77) Ye, T.; Gershgoren, E.; Friedman, N.; Ottolenghi, M.; Sheves, M.; Ruhman, S. *Chem. Phys. Lett.* **1999**, *314*, 429–434.

(78) Prokhorenko, V. I.; Nagy, A. M.; Brown, L. S.; Miller, R. J. D. *Chem. Phys.* **2007**, *341*, 296–309.

(79) Zgrablić, G.; Haacke, S.; Chergui, M. *Chem. Phys.* **2007**, *338*, 168–174.

(80) Dexheimer, S. L.; Wang, Q.; Peteanu, L. A.; Pollard, W. T.; Mathies, R. A.; Shank, C. V. *Chem. Phys. Lett.* **1992**, *188*, 61–66.

(81) Diller, R. In *Ultrashort Laser Pulses in Biology and Medicine*; Braun, M., Gilch, P., Zinth, W., Eds.; Springer: Berlin/Heidelberg, 2008; pp 243−277.

(82) Strambi, A.; Durbeej, B.; Ferré, N.; Olivucci, M. *Proc. Natl. Acad. Sci. U.S.A.* **2010**, *107*, 21322–21326.

(83) Petrich, J. W.; Breton, J.; Martin, J. L.; Antonetti, A. *Chem. Phys. Lett.* **1987**, *137*, 369–375.

(84) (a) Schoenlein, R. W.; Peteanu, L. A.; Wang, Q.; Mathies, R. A.; Shank, C. V. *J. Phys. Chem.* **1993**, *97*, 12087–12092. (b) Wang, Q.; Schoenlein, R. W.; Peteanu, L. A.; Mathies, R. A.; Shank, C. V. *Science* **1994**, *266*, 422–424.

(85) Birge, R. R.; Einterz, C. M.; Knapp, H. M.; Murray, L. P. *Biophys. J.* **1988**, *53*, 367–385.

(86) Polli, D.; Brida, D.; Manzoni, C.; Spillane, K. M.; Garavelli, M.; Kukura, P.; Mathies, R. A.; Cerullo, G. *Abstract of papers*; CLEO:2011—Laser Applications to Photonic Applications; Optical Society of America: Baltimore, MD, 2011; OSA Technical Digest (CD), paper JThB42.